Purely absorptive three-dimensional infrared spectroscopy

Garrett-Roe, S ; Hamm, P

Abstract: We demonstrate a method to collect purely absorptive three-dimensional (3D) fifth-order vibrational spectra on the model system CO2 in H2O. The six beam interferometer is described, as well as a method to experimentally determine the phase of the 3D spectrum. The measured spectra agree very well with simulations of the data based on the cumulant expansion. There are five peaks corresponding to different paths up and down the vibrational ladder. The positions, signs, and amplitudes of the peaks agree with theoretical predictions, and the intensities of the peaks scale linearly with concentration. Based on the concentration dependence and agreement between the simulations and measurements, we conclude that cascaded lower order signals contribute negligibly to the observed signal.

DOI: https://doi.org/10.1063/1.3122982

Purely absorptive three-dimensional infrared spectroscopy

Sean Garrett-Roe and Peter Hamm

Citation: The Journal of Chemical Physics **130**, 164510 (2009); doi: 10.1063/1.3122982
View online: http://dx.doi.org/10.1063/1.3122982
View Table of Contents: http://scitation.aip.org/content/aip/journal/jcp/130/16?ver=pdfcov
Published by the AIP Publishing

Purely absorptive three-dimensional infrared spectroscopy

Sean Garrett-Roe and Peter Hamm[a)]
Physikalish-Chemisches Institut, Universität Zürich, Winterthurerstr. 190, CH-8057 Zürich, Switzerland

(Received 20 January 2009; accepted 30 March 2009; published online 24 April 2009)

We demonstrate a method to collect purely absorptive three-dimensional (3D) fifth-order vibrational spectra on the model system CO_2 in H_2O. The six beam interferometer is described, as well as a method to experimentally determine the phase of the 3D spectrum. The measured spectra agree very well with simulations of the data based on the cumulant expansion. There are five peaks corresponding to different paths up and down the vibrational ladder. The positions, signs, and amplitudes of the peaks agree with theoretical predictions, and the intensities of the peaks scale linearly with concentration. Based on the concentration dependence and agreement between the simulations and measurements, we conclude that cascaded lower order signals contribute negligibly to the observed signal. © *2009 American Institute of Physics*. [DOI: 10.1063/1.3122982]

I. INTRODUCTION

Nonlinear vibrational spectroscopy is a rapidly developing set of experimental techniques. Third-order spectroscopies such as absorptive two-dimensional infrared spectroscopy (2D-IR) have become a standard way to measure the dynamics of vibrational chromophores,[1–3] chemical exchange,[4–7] couplings between vibrations,[8] vibrational coherence transfer,[9,10] and many other phenomena.[11] Fifth-order vibrational spectroscopies are much newer; they should be useful to investigate non-Gaussian frequency fluctuations,[12] probe higher vibrational states,[13] and better characterize the anharmonic vibrational potentials.[14] For example, Ding and Zanni[15] recently demonstrated a fifth-order experiment which used a pulse sequence with three coherence times (one of which was a two-quantum coherence), making it a three-dimensional infrared (3D-IR) spectroscopy. They showed how this can increase the effective spectral resolution, decreasing spectral congestion, by spreading the many vibrational signals over three frequency dimensions. This technique also allows one to look higher up the vibrational ladder at the $v=2-3$ transition anharmonicity and lineshape.

Historically, two-dimensional infrared (2D-IR) spectra have been presented in several of different ways—real and imaginary components of rephasing and nonrephasing spectra, or absolute value spectra. Each of these experiments is related to measuring a specific Liouville space pathway, which can contain useful information, for example, in isolating signatures of coherence transfer[9,14,16,17] and vibrational frequency correlations.[18] Purely absorptive 2D-IR spectra, which are the real part of the sum of rephasing and nonrephasing spectra, were introduced somewhat later[19] in analogy to NMR,[20] but have proved very useful. First, these spectra give the highest spectral resolution. Each positive or negative feature corresponds to a specific vibrational band, whereas rephasing and nonrephasing spectra contain several positive and negative lobes. Also, an absorptive lineshape is narrower because the long range, dispersive components have been eliminated. These two factors both reduce spectral congestion. Another consideration is that absorptive spectra are at the level of electric field measurements, so the signals are additive, whereas absolute magnitude spectra can contain the effects of interferences between signals. Finally, the absorptive spectra are easier to interpret because they can be related to the frequency trajectories and correlation functions more directly than either the rephasing or nonrephasing spectra individually.[12]

Because an absorptive spectrum comes from the addition of rephasing and nonrephasing spectra, which, in turn, come from different pulse orderings, an absorptive fifth-order measurement must have five independently controllable pump beams and involve all one quantum coherences. The 3D-IR experiments of Ding and Zanni[15] used three independent pump fields which required the system to have multiple interactions with the same pump laser fields. The spectra therefore cannot be transformed into a completely absorptive spectrum.

In this report, we demonstrate experimentally how these ideas from 2D spectroscopy can be extended to fifth-order vibrational spectroscopy—a purely absorptive 3D-IR spectrum of CO_2 dissolved in H_2O. The CO_2 molecule has a large extinction coefficient [$\sim 1000\ M^{-1}\ cm^{-1}$ (Ref. 21)] and a narrow linewidth, $\sim 7\ cm^{-1}$, which is almost entirely homogeneously broadened,[22,23] making it an excellent model compound to characterize the spectroscopy. For this system the agreement between the measured spectrum and simulations based on the cumulant expansion[24] truncated at second order is excellent. We demonstrate that summing the four experiments corresponding to the four Feynman diagrams $R^{(5)}_{1-4}$ (Fig. 1) leads to a purely absorptive spectrum. For a multilevel, anharmonic oscillator such as CO_2, there are five peaks in the 3D-IR spectrum corresponding to different paths up and down the vibrational ladder. The amplitudes and signs of these peaks match analytical estimates based on harmonic scaling of the transition dipole moments. We demonstrate that the method used to determine the absolute phase of a

[a)]Electronic mail: phamm@pci.unizh.ch.

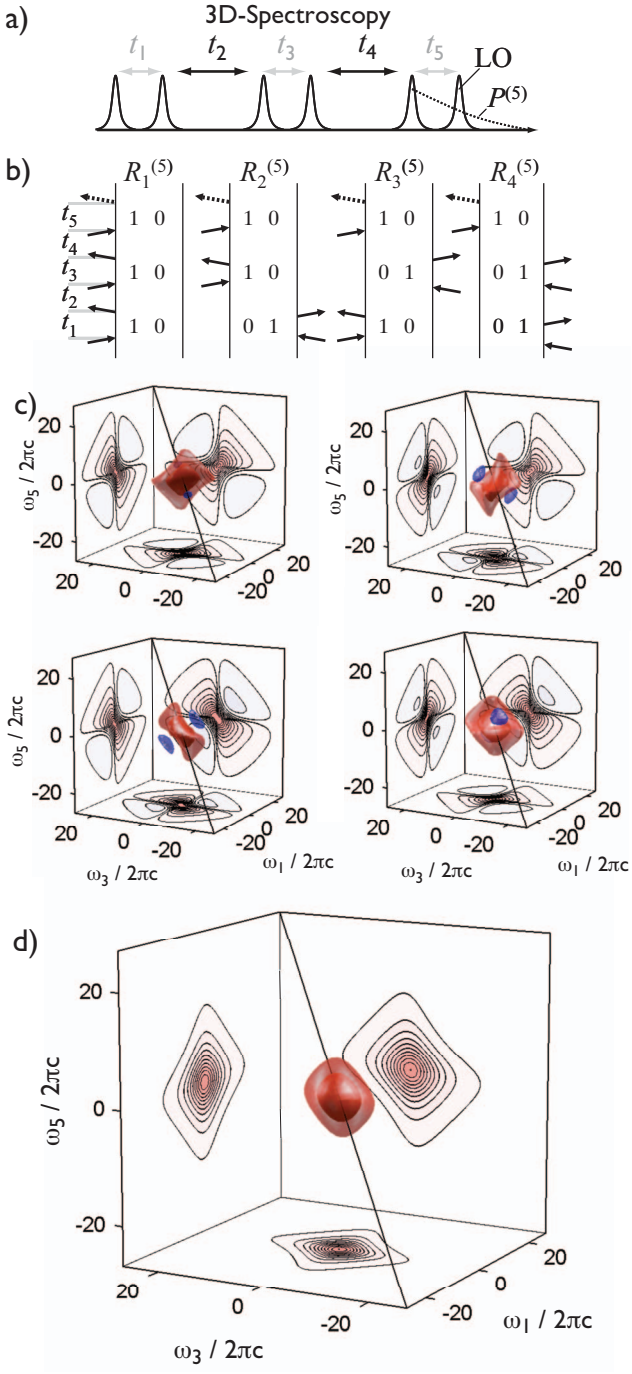

FIG. 1. (Color) (a) Fifth-order, 3D spectroscopy has five strong pump pulses which generate a fifth-order polarization, $P^{(5)}$ which interferes with a local oscillator, LO. (b) The four double-sided Feynman diagrams for the phase matching direction $k_s=k_1-k_2+k_3-k_4+k_5$ for a two-level system. (c) The signal from each of these diagrams alone has a phase-twisted lineshape. (d) Adding these four diagrams generates an absorptive fifth-order spectrum.

2D-IR experiment[25] can be extended in a straightforward fashion to measure the phase of a 3D spectrum. Finally, we discuss the possibility of cascaded third-order signals in the 3D spectrum, and conclude that cascaded signals can comprise no more than a few percent of the signal.

II. MATERIALS AND METHODS

Ultrafast 800 nm pulses are generated by a commercial Ti:sapphire oscillator and chirped pulse amplifier (Spectra-Physics), making 1 mJ pulses at a 1 kHz repetition rate. This pumps a homebuilt optical parametric amplifier[26] (OPA), which generates 1.8 μJ of tunable midinfrared with 150 cm^{-1} of bandwidth.

The IR from the OPA then enters the 3D-IR interferometer (Fig. 2). The IR is overlapped with a 5 mW HeNe (Melles Griot) by means of a Ge window. The input beams are then divided successively into pairs by custom coated BaF_2 windows (Laseroptik) coated with the appropriate reflection coefficients for the IR and visible. The BaF_2 windows are wedged at 0.6° to spatially separate ghost reflections. The local oscillator (LO) is separated by the ~4% Fresnel front reflection from an uncoated BaF_2 window. The reflection from the back face is sent in the phase matching direction and is used as a tracer beam for alignment purposes. Before entering the sample stage, approximately 50% of the HeNe is separated from the IR by a custom 8 mm thick, 150 mm wide ZnSe window (Laser Optex) set at Brewster's angle for the IR. The reflected HeNe is used for active feedback,[27] while the transmitted component is used for alignment at the sample. The interferometer is actively phase stabilized using the interference pattern between the HeNe tracers in each a pair of beams. The feedback signal drives mirrors mounted on piezos (P1–P3) (Piezomechanik HPSt 150/20-15/12 VS35) which controls the optical path length. The HeNe also acts as an internal calibration of the position of the delay stages. The stepper motors (Thorlabs ZST25B) have substantial systematic errors as a function of the lead screw pitch, which we correct with the piezos. The dispersion of each beam is balanced with appropriate compensation plates. Each beam can be opened or closed by a computer controlled mask without interrupting the phase feedback so that the phasing procedure (Sec. III) can be automated.

We use the balanced detection method proposed by Fulmer *et al.*[28] In our case, the LO passes through the sample with the other pulses with a small vertical offset (−15 mm) from the phase matching direction [Fig. 2(b)]; after the sample stage the LO runs 15 mm above the emitted fifth-order polarization, $P^{(5)}$. The LO overlays the $P^{(5)}$ on opposite sides of 50% beamsplitter [Fig. 2(c)]. Half of the fifth-order polarization passes through the beamsplitter, and half reflects off the front face of the beamsplitter. Because this is an external reflection, the field experiences a 180° phase shift. The LO also crosses the beamsplitter; half passes through, and half undergoes an *internal* reflection so there is *no* phase shift. When the LO and $P^{(5)}$ overlap in the spectrometer, they generate two signals with opposite signs measured on the two lines of the array detector, S_1 and S_2, respectively. The balanced detector is outside of the phase-stabilization loop. Over the time course of the experiments, however, the phase drift introduced by this one set of optics is less than 5° based on spectral interferometry of each pair of beams diffracting off a pinhole.

Scattered light from pump beams 1-4 is removed by measuring the light with and without the fifth pump (with a 500 Hz chopper). When the fifth pump is blocked, the two lines of the array detector measure signals S_3 and S_4. Scattered light from the last pump, as well as pump-probe signal,

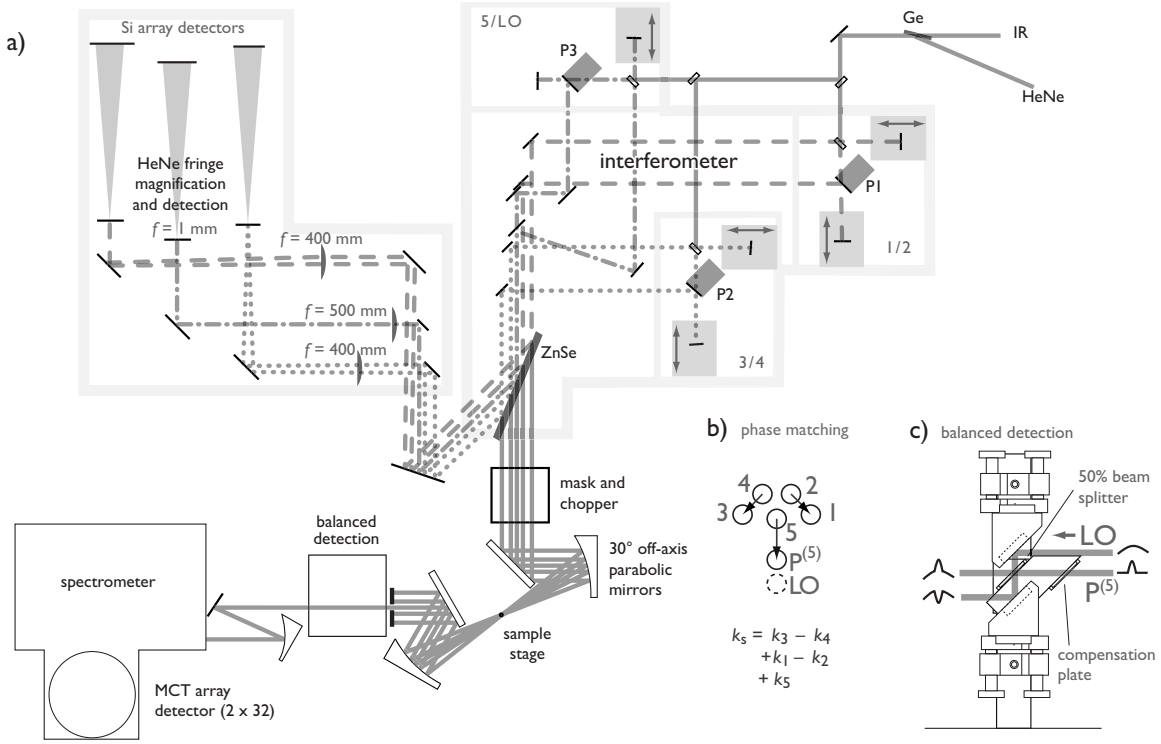

FIG. 2. Schematic of the six beam interferometer for 3D-IR spectroscopy. (a) interferometer layout, (b) phase matching geometry, and (c) balanced detection.

is independent of the delay between the pumps 1-2 and 3-4, so it is removed by the 2D Fourier transforms of t_1 and t_3. The final signal is then

$$I = -\log\left(\frac{S_1 S_4}{S_2 S_3}\right),$$

which is effectively an absorption scale which corrects the measured spectrum for the spectrum of the LO, though the other two frequency axes, ω_1 and ω_3 are uncorrected.

The cuvette is made of 2 mm thick CaF_2 windows, separated by a 6 μm Mylar spacer. The sample must be so thin because of the residual H_2O absorption, due to the wing of the water combination mode centered at $\sim$2100 cm^{-1}. The sample is carbonated water, $[CO_2]=0.08\pm0.02$ M. The peak optical absorption is $\sim$0.16 outside diameter [Fig. 3(b)] around the CO_2 asymmetric stretch (centered at 2344 cm^{-1}) to prevent excessive distortion of the input pulses as they propagate through the sample. The cuvette is configured as a flow cell[29] so that the fluid can be replaced, which is necessary because the CO_2 outgasses on a few hour time scale.

The experimental phase matching geometry [Fig. 2(b)] is adapted from fifth-order Raman measurements, and will be discussed in Sec. VI. The laser pulses are focused on the sample by 3 in. diameter, 30° off-axis parabolic mirrors (Janos) with an effective focal length of 123 mm.

The interferograms as a function of t_1 and t_3 were collected at two resolutions, 10 cm^{-1} (31 steps of 109.7 fs, undersampling 15 times, 1.5 h total time) and 5 cm^{-1} (41 steps of 166.7 fs, undersampling 23 times, 2.8 h total time, data not shown). The 300 l/mm grating provides a 3 cm^{-1} resolution in the directly detected dimension ω_5. The interferograms are apodized (triangular) and zero-padded (128 points) after baseline correction. The first point of the interferograms is scaled by a factor of 0.5 before Fourier transformation as noted in processing NMR free induction decays[30] in order to eliminate a base line artifact from the discrete Fourier transformation of a single sided function.

III. PHASING OF FIFTH-ORDER SIGNALS

Noncollinear, heterodyne detected third-order spectroscopy is a phase-sensitive measurement in which the phase

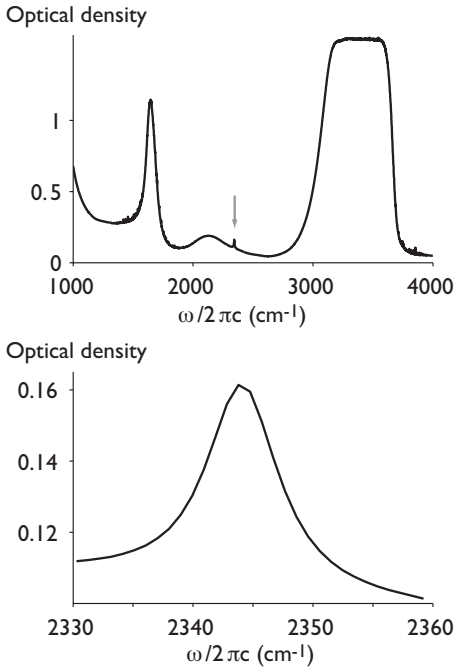

FIG. 3. Absorption spectrum of CO_2 in H_2O; the sample path length is 6 μm.

between optical pulses must be known to a fraction of the wavelength. Most 2D spectra collected to date have corrected the phase of the spectrum to match the projection of the spectrum to a broadband pump-probe experiment in a postprocessing step.[31] This phase can be experimentally determined,[25,32] however, and here we extend the method of Backus *et al.*[25] to fifth-order spectroscopy. It is especially important to have a direct determination of the pulse phase because the postprocessing to correct the phase of a 3D spectrum would be based on like a broadband pump 2D-IR probe experiment, which itself would require phasing.

The concept we use to experimentally determine the phase is based on a transient-grating description of the nonlinear spectroscopy. Essentially, each pulse pair, 1-2, 3-4, and 5-LO, generates a spatial interference pattern—a grating—in the focal plane of the sample that the other pump beams can scatter off. The distance between the maxima of the spatial interference pattern is proportional to the inverse of the wavevector difference. For beam pair 1-2, for example, the fringe spacing is

$$\Delta \mathbf{x}_{12} = 1/(\mathbf{k}_1 - \mathbf{k}_2).$$

A phase shift in beams 1 or 2 would shift this spatial grating. In 2D spectroscopy, the phase matching condition is $k_s = k_2 - k_1 + k_3$ or $k_{\mathrm{LO}} - k_5 = k_2 - k_1$, which implies that the signal will be correctly phased when the two spatial interference patterns align in the focus.

Bristow *et al.*[32] demonstrated measuring these spatial interference patterns directly with a microscope objective and a beam profiler, which is feasible in the visible and near-IR. In the mid-IR, however, high pixel count 2D arrays are not available and one needs to use an additional trick. We sample the spatial interference patterns with a very small pinhole, roughly the size of the wavelength of light. The diffraction from two beams off the pinhole we measure as a function of the time delay between the two pulses. The diffraction converts the spatial interference pattern into a temporal one. We Fourier transform the measured interference patterns to find their magnitude and phase as a function of frequency. The magnitude spectrum reproduces the input spectrum of the laser beam, and the phase as a function of frequency we further analyze.

The phase as a function of frequency allows us to determine the correct timing of the pulses and determine any residual phase. As others have noted,[33] in experiments that use delay stages to shift phases, the pulse phase and the delay are coupled. Moving a time delay of a pulse changes both the phase and shifts the carrier envelope, which creates a linear phase shift as a function of frequency

$$\frac{d\phi}{d\omega} = \frac{dt}{2\pi}.$$

Here, we resolve this ambiguity by using the linear slope of the phase with respect frequency to temporally overlap the pulse envelopes as best as we can—our active phase locking scheme restricts us to time steps of one period of a HeNe, ~2.11 fs. The residual phase extracted from the interferograms is used to "rephase" the data.

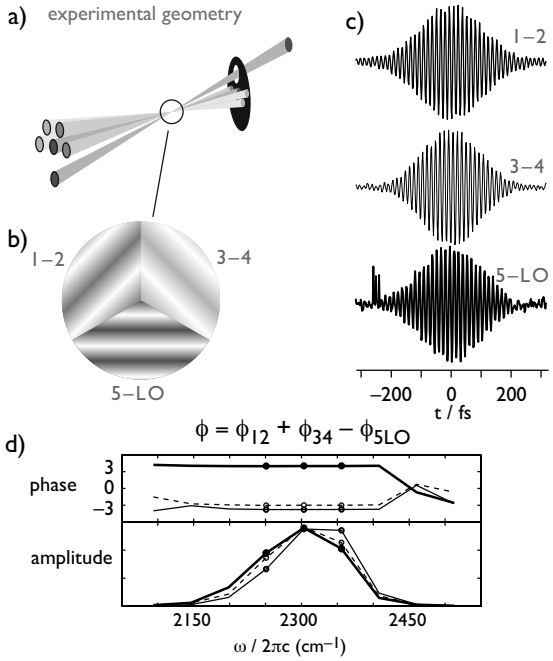

FIG. 4. Phasing fifth-order signals. (a) Each pair of beams that creates a coherence in the sample also creates (b) a spatial grating in the focus. (c) A small pinhole, 5 μm diameter, diffracts some of these gratings in the direction of the detector, converting the spatial grating to an interferogram. (d) The phases from the Fourier transforms of these interferograms can be used to calculate the phase of the 3D-IR spectrum.

In a 3D-IR measurement, there are three sets of interference patterns to measure (Fig. 4). Our phase matching geometry [Fig. 4(a)] means that each pair of pump pulses generates a spatial interference pattern [Fig. 4(b)]. Each colored pattern represents a small area of the spatial interference patterns when only one pair of beams is present. These patterns indicate schematically the spacing and orientation of the interference patterns. Unlike the 2D case in a boxcar geometry, these spatial interference patterns are tilted with respect to each other. The small pinhole diffracts light into the direction of a spectrally integrating detector (i.e., one pixel of our array when the grating is at the zero-order diffraction angle). These interference patterns as a function of the coherence time [Fig. 4(c)] then can be Fourier transformed [Fig. 4(d)] and analyzed. The phase matching condition for 3D spectroscopy implies that the spectra depend on $\phi_{12} + \phi_{34} - \phi_{5,\mathrm{LO}}$.

IV. ABSORPTIVE FIFTH-ORDER SIGNALS

In a heterodyne detected fifth-order experiment, there are five interactions with the pump laser fields as well as a weak LO which interferes with the emitted fifth-order polarization on the detector [Fig. 1(a)]. By placing the detector in the phase matching direction $k_s = k_1 - k_2 + k_3 - k_4 + k_5$ we select diagrams such as $R^{(5)}_{1-4}$ [Fig. 1(b)]. This pulse sequence has three coherence times t_1, t_3, and t_5 and two population times t_2 and t_4. Because each interaction is from a separate beam, we can control each of these experimental parameters. For a two-level system there are four possible diagrams corresponding to having the density matrix in either the coherence $|0\rangle\langle 1|$ or $|1\rangle\langle 0|$ during t_1 and t_3.

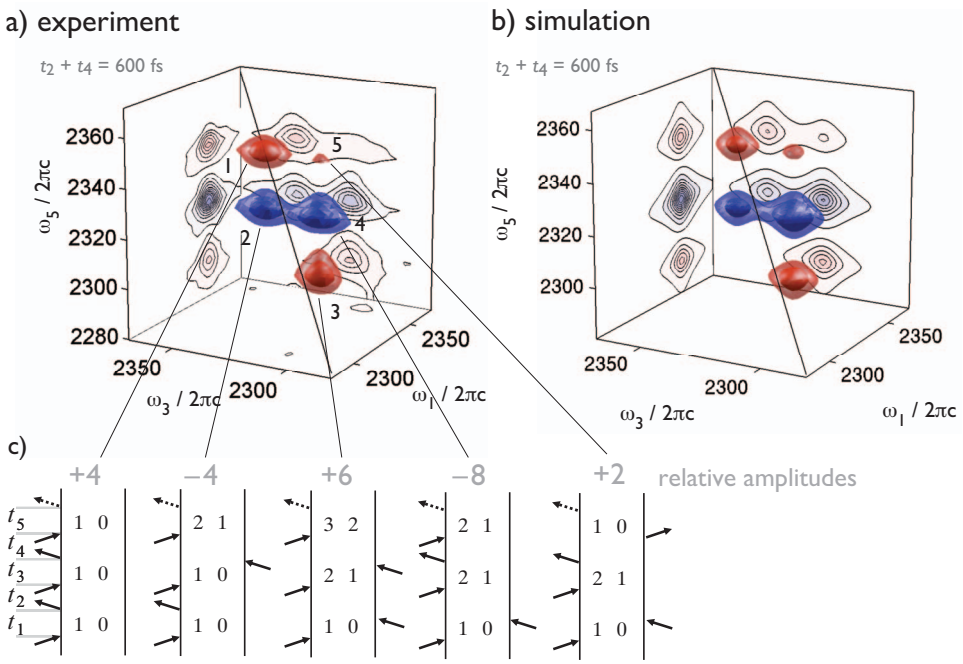

FIG. 5. (Color) (a) The experimental absorptive 3D spectrum of CO_2/H_2O gives five peaks ($t_2=t_4=300$ fs). (b) Simulations based on the cumulant expansion accurately reproduce the data. (c) The five peaks come from the various pathways up and down the vibrational ladder. Above each column in gray are the relative amplitude and sign of each peak accounting for the various pathways through population states and harmonic scaling of the transition dipole moments.

The signal from each diagram alone has a phase-twisted lineshape. That is, the real part of the response functions from a two-level system have complicated 3D shapes [Fig. 1(b)]. The real component of the sum of these diagrams, however, has a much simpler overall structure. The peak is much more compact [Fig. 1(d)], and these spectra are easier to interpret.[12]

The signals from these four diagrams must collected under identical conditions and then be added to produce a purely absorptive 3D-IR spectrum. The basic idea of an absorptive spectrum is that in a pump-probe measurement, the system interacts with the pump field two times—once on the bra and once on the ket, which can come in either order. One necessarily measures the sum of both time orderings, because there is no way to separate the interactions—they occur with the same laser pulse. In an echo experiment, however, these two interactions happen with different laser fields, so one must add signals from the two possible time orderings in order to recover a spectrum with absorptive features.[19] In the fifth-order case, there are then two time orderings for each of two pump pairs, or a total of four different pulse orderings that must be measured.

V. RESULTS

For a two-level system, there would be only one peak in the 3D spectrum (Fig. 1). An anharmonic oscillator such as CO_2, however, gives rise to five peaks corresponding to the various pathways up and down the vibrational ladder (Fig. 5). For example, the first diagram [Fig. 5(c) far left] corresponds to all coherences occurring between the ground and first excited states. During the population times t_2 and t_4, the system could go through either the population state $|0\rangle\langle 0|$ or through $|1\rangle\langle 1|$ leading to four possibilities, indicated in gray over the diagram. For the excitations to higher-lying vibrational states, there is an additional consideration. The transition dipole moment increases with vibrational quantum number; we use the scaling rules of a harmonic oscillator ($\mu_{21}=\sqrt{2}\mu_{01}$ and $\mu_{32}=\sqrt{3}\mu_{01}$) to treat this effect. In this way, each of the coefficients above the diagrams [Fig. 5(c)] represents the number of ways the system can pass through the given coherences by way of the various population states scaled by the transition dipole strength.

The experimental 3D-IR spectra [Fig. 5(a)] agree very well with simulations of the spectra using the cumulant expansion truncated at second order [Fig. 5(b)]. The low-resolution spectrum (10 cm^{-1}) is shown. In general, the lineshape depends on the details of the two-point frequency fluctuation correlation function, but in agreement with previous third-order experiments,[22,23] we find that the dynamics are in the Bloch limit, and are almost completely homogeneously broadened; the linewidth is 7 cm^{-1}. These simulations include the effects of the loss of rotational correlation due to rotational diffusion of the molecules,[14,34,35] although the influence on the lineshape is minor. This level of theory reproduces the number, amplitude, sign, and spacing of the experimental peaks.

Visual inspection of Fig. 5 shows the qualitative agreement of the measured and simulated spectra. The amplitudes of the peaks do not exactly match the simple estimate based on the harmonic scaling of the dipole moments (Table I), largely due to the overlap and partial cancellation of the bands. Taking this into account, as well as the smaller effects of the finite frequency resolution, loss of rotational correlation, and the finite bandwidth of the laser, the simulations and experiments agree very well. The largest deviation is the measured amplitude of peak 4 (Table I), which is the strongest band in the spectrum, and is too small by 20%. One assumption in these simulations is that the dynamics between the different vibrational states are perfectly correlated, however, it is very common to see lineshape differences in

TABLE I. A comparison of the amplitude of the five detected peaks with the analytical results assuming a harmonic scaling of the transition dipole moments, simulation, and experiment. The simulation of the signals uses the cumulant expansion and the same time grid as the experiment. The coherence pathways correspond to reading the bra-ket pairs going up the double-sided Feynman diagrams of Fig. 5.

Coherence harmonic			10 cm^{-1} res.		5 cm^{-1} res.	
Peak	pathway	scaling	Simulation	Experiment	Simulation	Experiment
1	10|10|10	1.0	1.0	1.0	1.0	1.0
2	10|10|21	−1.0	−1.1	−0.9	−1.1	−1.0
3	10|21|32	1.5	1.3	0.8	1.2	1.1
4	10|21|21	−2.0	−1.8	−1.2	−1.9	−1.5
5	10|21|10	0.5	0.4	0.4	0.4	0.3

2D-IR spectra. Generally the higher-lying vibrational states are broader causing more cancellation and reduced observed intensity compared to the ground state bleach and stimulated emission.

The largest difference between the experiment and the simulation is that in the ω_5 direction, the peaks are not exactly equally spaced. This is most visible in the projection of the 3D spectrum onto the $\omega_1-\omega_5$ plane. The Morse oscillator predicts that the difference in the transition frequencies of the $v=0-1$ and $v=1-2$ states, $\Delta^{(1)}=\omega_{01}-\omega_{12}$, should be the same as the difference between the frequencies of the $v=1-2$ and $v=2-3$ transitions, $\Delta^{(1)}=\Delta^{(2)}$ where $\Delta^{(2)}=\omega_{12}-\omega_{23}$. Few experiments can measure $\Delta^{(2)}$, but recent fifth-order experiments[13,15] showed that aside in an ionic glass deviates from the Morse form, with $\Delta^{(2)}=\Delta^{(1)}+4$ cm^{-1}. Here, for the nonionic CO_2 in liquid water, find that $\Delta^{(2)}=\Delta^{(1)}+2$ cm^{-1}.

The intensity of the measured signals is linear with the concentration of CO_2 (Fig. 6). These intensities are determined by dilution of a stock solution, whose concentration was estimated to be 0.08 ± 0.02 M^{-1} cm^{-1}. Here the large error bar reflects the difficulty in reproducibly establishing the concentration. The concentration series, however, is made by diluting the same stock solution, so the error in concentration should be highly correlated and not reflect random scatter. We measured the intensity from the peak-to-peak height of the time-domain interferogram at two wavelengths ($\omega_5=2320$ and 2344 cm^{-1}) near $t_1=t_3=0$ fs.

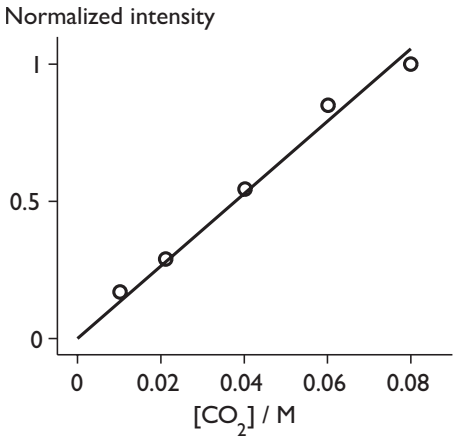

FIG. 6. The intensity of the measured signal is linear with concentration, c. Direct fifth-order signal should be linear with c, whereas cascaded third-order signals should scale like c^2. This indicates that cascaded third-order signals do not contribute to the 3D-IR.

VI. CASCADING THIRD-ORDER SIGNALS DO NOT CONTRIBUTE TO THE FIFTH-ORDER IR SPECTRUM

Any new higher-order nonlinear spectroscopy has to discuss the possibility of cascading third-order signals because they had such an impact on the fifth-order Raman measurements. Early fifth-order Raman experiments[36–38] were contaminated by contributions of undesired, cascaded third-order signals[39–41] (and references in the review by Kubarych *et al.*[42]). A cascade is a process involving two third-order excitations, one of which can be emitted and absorbed by another chromophore in the sample. Essentially, one third-order signal acts as to pump or to stimulate another third-order process along with the two other external fields. These cascades are very difficult to separate from the desired fifth-order signal. They emerge in the same phase matching direction; they depend on all of the pump fields so have the same intensity scaling. Third- and fifth-order signals do scale differently with sample concentration, and the cascaded signal is 90° out of phase with the fifth-order signal due to the extra electric field interaction. Recent experiments have been able to measure pure fifth-order Raman signals by suppressing the third-order cascades by careful choice of the phase matching geometry, optimized optical path length, and heterodyne detection.[42,43] In this section we will show that the contrast mechanisms that were used to suppress cascades in the fifth-order Raman—phase matching and phase-sensitive detection—do not discriminate fifth-order signal from cascades in the IR. Nevertheless, we will show that the cascading third-order signals are not a problem for the fifth-order IR experiments, in agreement with the earlier conclusion of Fulmer *et al.*[44] because all of the transitions are allowed one quantum transitions, where fifth-order Raman has a forbidden step.

There are some differences between the fifth-order IR and Raman experiments. For instance, we chose the "baseball diamond" phase matching geometry, which carries most of the benefits of the "Dutch Cross," because these geometries had been very important for the Raman measurements.[42] The best phase matching geometry discovered so far, the so called Dutch Cross, suppresses the third-

order signal not by sending it in a different direction, which is impossible, but by maximizing the phase mismatch as the cascading signal propagates through the sample. In the thick film limit, efficiency of signal generation depends on the angle between the pump beams. The Dutch Cross geometry suppresses cascades by maximizing the angles involved in the cascaded signals. In contrast to the Raman experiments, however, the experiments we have reported here are done in the thin film limit. The sample thickness, l, is comparable to the wavelength of light, λ. As such, the sample makes an effectively 2D grating, and the phase matching (in the signal propagation direction) used in the Raman experiments to suppress cascades does not work here. In the thin film limit, the efficiency of the nonlinear processes is nearly independent of the angle between the incoming beams, so these techniques are not effective at suppressing cascaded signals. In retrospect, we now believe that many other phase matching geometries will be successful in the IR regime.

The phase dependence is another consideration. In the Raman, the cascaded signals are 90° out of phase with the direct fifth-order signal but in the IR they are 180° out of phase. In both the Raman and IR, the direct and cascaded signals are proportional to

$$S^{(5)} \propto iR^{(5)}E_1E_2E_3E_4E_5, \tag{1}$$

$$S^{(5)}_{\mathrm{cas}} \propto i^2R^{(3)}R^{(3)}E_1E_2E_3E_4E_5. \tag{2}$$

Every time a polarization is converted to an emitted field it generates a factor of i. The direct signal has one radiation event, the emitted field, and the cascade has two, the emission of the intermediate field and the final emitted signal.[45] In the Raman, $R^{(5)}$ and $R^{(3)}$ are real valued so the signals differ by one factor of i and are 90° phase shifted. In the IR, however, $R^{(5)}$ and $R^{(3)}$ are imaginary, $R^{(5)} \propto i^5$ and $R^{(3)} \propto i^3$, so $S^{(5)}$ and $S^{(5)}_{\mathrm{cas}}$ differ by two factors of i and are 180° phase shifted.

In general, these phase factors are complicated functions of the detuning of the pump fields from any nearby resonances.[24] The IR and Raman, however, can be treated as two extreme cases, namely, resonant and off-resonant. In linear spectroscopies, the resonant interactions generate in-phase signal fields (absorption or dichroism) which destructively interfere with the probe beam; the dispersive interactions generate in-quadrature signal fields (birefringence).[24,46] For on-resonance nonlinear spectroscopies, such as pump-probe spectroscopy, the third-order emitted field is in phase, constructively (bleach and stimulated emission) or destructively interfering (excited state absorption) with the probe field. On the other hand, in transient birefringence measurements (the optical Kerr effect) the signal field is shifted 90° with respect to the last interaction.[47]

Fifth-order Raman measurements using diffractive optics[42] use phase as a contrast mechanism. The relative phase of the pulses is determined by the design of the diffractive optic. Our phasing procedure serves a similar role and makes the phase an experimentally determined factor and not a free parameter. We can use the relative sign of the five peaks to see if the signals are cascaded or not, but phase contrast in the IR cannot suppress the cascades relative to the fifth-order signal.

The physical picture behind a cascaded third-order signal is that the first laser pulses generate a third-order polarization which can pump or stimulate another third-order process. At this level of description, a third-order signal must compete as a pump field with the laser pulses, but, as long as the perturbative limit holds—i.e., only a fraction of the sample is excited, about 0.12 in this work—the third-order signal is much smaller than the incoming pulses that generate it. In the Raman, the cascades *can* compete because the cascaded third-order signals involve all allowed (one quantum) transitions. On the other hand, restricting the number of field interactions to five necessarily implies that one of the direct fifth-order Raman interactions is a two-quantum transition, which would be forbidden in the harmonic case, and becomes only weakly allowed in the presence of anharmonicity. In other words, Raman combination bands and overtones are weak transitions. The forbidden nature of this step is what makes the fifth-order Raman signal weak enough that the cascades can effectively compete with them. There are additional factors in the ratio of cascaded to direct fifth-order signal $|S_{\mathrm{cas}}|/|S^{(5)}|$, which have been discussed in detail by Fulmer *et al.*[44] for fifth-order IR and reviewed by Kubarych *et al.*[42] for fifth-order Raman. One important weighting function is phase matching factor, but in the thin film limit of these experiments, these factors are all close to unity. The next important terms in resonant experiments together scale like the total optical density of the sample. For this reason, the relative amplitude of cascaded signal could become larger in optically thick samples.

Experimentally, it is clear that the 3D-IR signals (Fig. 5) are not entirely due to cascades because cascaded third-order interactions could not generate the observed five peaks (Fig. 7). Sequential and parallel cascades could generate 2 of the 5 peaks [Figs. 7(a) and 7(b)]. Sequential cascades could potentially contribute to two more peaks [Figs. 7(c) and 7(d)] but these signals involve transferring coherence from $|2\rangle\langle 1|$ to $|1\rangle\langle 0|$ coherences during t_3. For the present case, the separation between the bands will strongly suppress this pathway. Finally, no cascade could generate the most redshifted peak [Fig. 7(e)]. This peak comes from upclimbing the vibrational ladder, reaching the $v=2 \rightarrow v=3$ transition. This is possible only in fifth-order spectroscopy; the maximum in third-order spectroscopy is $v=1 \rightarrow v=2$ even if the signal is generated by a cascade.

If direct and cascaded processes were of similar magnitude, then cascaded signals could destructively interfere with the pathways [Figs. 7(a) and 7(b)] that involve only 0-1 and 1-2 coherences. That the signs and amplitudes of the measured 3D-IR match the simulations reasonably well is evidence that cascading third-order signals are not important for the 3D-IR; this argument, however, rests on the assumption of harmonic scaling of the transition dipole moments, which is a weak assumption. The harmonic scaling laws are only an approximation, and their inaccuracy could conceal some cascaded signal.

Most importantly, the 3D-IR signal intensity is linear in

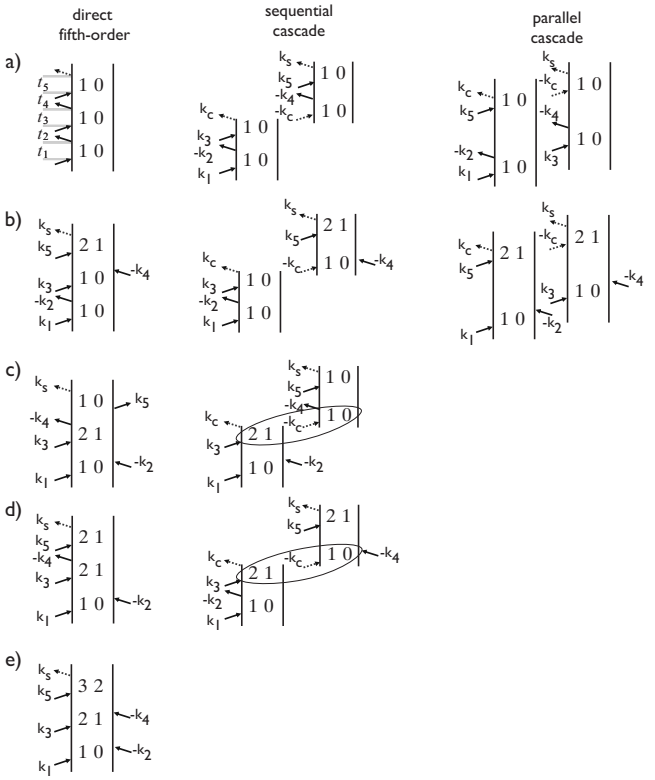

FIG. 7. The double-sided Feynman diagrams for cascaded third-order signals. The left column gives the diagrams for direct fifth-order processes which generate the five peaks in the 3D-IR spectrum. The middle column gives the sequential cascaded processes in which one chromophore emits a field which acts as a pump for another third-order process on another chromophore. The right column gives the parallel cascades, in which a third-order process on one chromophore stimulates the emission of a third-order process on another chromophore. [(a) and (b)] For these two peaks cascaded processes exist to generate signals. [(c) and (d)] For these two peaks there is a sequential cascade (but no parallel cascade) which could potentially generate a signal at these frequencies. It will be suppressed by the frequency mismatch between the $|2\rangle\langle 1|$ and $|1\rangle\langle 0|$ coherences, which are circled. (e) There is no cascade which can generate this peak because it requires walking up the vibrational ladder.

the concentration of CO_2 (Fig. 6), as noted earlier in the fifth-order IR measurements by Fulmer *et al.*[44] Direct fifth-order signals scale linearly with concentration and path length, cl, but cascaded signals, which necessarily involve two chromophores, scale like c^2l^2. The linear concentration dependence (Fig. 6) allows us to conclude that cascaded signals contribute negligibly to these measurements.

VII. CONCLUSIONS

We have demonstrated the experimental basis for collecting purely absorptive 3D-IR spectra. The spectra from CO_2/H_2O agree with simulations based on the cumulant expansion truncated at second order, and the signal intensity is linear with concentration, allowing us to conclude that cascaded third-order signals cannot contribute more than a few percent of the observed signal. Based on these observations, 3D-IR spectroscopy can be applied to more complex systems. The basic NMR pulse sequences NOESY and COSY are basically equivalent to 2D-IR spectroscopy, but the success of NMR has largely been based on much more complicated pulse sequences. This work represents a step in that direction for IR spectroscopy.

ACKNOWLEDGMENTS

The work was supported by the Swiss Science Foundation under Grant No. 200020-107492/1. S.G.-R. was partially supported by the National Science Foundation (USA) under Grant No. OISE-0601907.

[1] J. B. Asbury, T. Steinel, C. Stromberg, S. A. Corcelli, C. P. Lawrence, J. L. Skinner, and M. D. Fayer, J. Phys. Chem. A **108**, 1107 (2004).
[2] J. D. Eaves, J. J. Loparo, C. J. Fecko, S. T. Roberts, A. Tokmakoff, and P. L. Geissler, Proc. Natl. Acad. Sci. U.S.A. **102**, 13019 (2005).
[3] S. T. Roberts, J. J. Loparo, and A. Tokmakoff, J. Chem. Phys. **125**, 084502 (2006).
[4] S. Woutersen, R. Pfister, P. Hamm, Y. G. Mu, D. S. Kosov, and G. Stock, J. Chem. Phys. **117**, 6833 (2002).
[5] J. R. Zheng, K. Kwak, J. Asbury, X. Chen, I. R. Piletic, and M. D. Fayer, Science **309**, 1338 (2005).
[6] J. R. Zheng, K. W. Kwak, J. Xie, and M. D. Fayer, Science **313**, 1951 (2006).
[7] Y. S. Kim and R. M. Hochstrasser, Proc. Natl. Acad. Sci. U.S.A. **102**, 11185 (2005).
[8] M. Khalil, N. Demirdöven, and A. Tokmakoff, J. Phys. Chem. A **107**, 5258 (2003).
[9] M. Khalil, N. Demirdöven, and A. Tokmakoff, J. Chem. Phys. **121**, 362 (2004).
[10] M. J. Nee, C. R. Baiz, J. M. Anna, R. McCanne, and K. J. Kubarych, J. Chem. Phys. **129**, 084503 (2008).
[11] R. M. Hochstrasser, Proc. Natl. Acad. Sci. U.S.A. **104**, 14190 (2007).
[12] P. Hamm, J. Chem. Phys. **124**, 124506 (2006).
[13] E. C. Fulmer, F. Ding, P. Mukherjee, and M. T. Zanni, Phys. Rev. Lett. **94**, 067402 (2005).
[14] F. Ding, E. C. Fulmer, and M. T. Zanni, J. Chem. Phys. **123**, 094502 (2005).
[15] F. Ding and M. T. Zanni, Chem. Phys. **341**, 95 (2007).
[16] G. S. Engel, T. R. Calhoun, E. L. Read, T. K. Ahn, T. Mancal, Y. C. Cheng, R. E. Blankenship, and G. R. Fleming, Nature (London) **446**, 782 (2007).
[17] A. V. Pakoulev, M. A. Rickard, N. A. Mathew, K. M. Kornau, and J. C. Wright, J. Phys. Chem. A **112**, 6320 (2008).
[18] N. H. Ge, M. T. Zanni, and R. M. Hochstrasser, J. Phys. Chem. A **106**, 962 (2002).
[19] M. Khalil, N. Demirdöven, and A. Tokmakoff, Phys. Rev. Lett. **90**, 047401 (2003).
[20] R. R. Ernst, G. Bodenhausen, and A. Wokaun, *Principles Of Nuclear Magnetic Resonance in One and Two Dimensions* (Oxford University Press, New York, 1987).
[21] G. Moore, A. Chizmeshya, and P. F. McMillan, Geochim. Cosmochim. Acta **64**, 3571 (2000).
[22] P. Hamm and R. M. Hochstrasser, in *Ultrafast Infrared and Raman Spectroscopy*, edited by M. D. Fayer (Dekker, New York, 2001), p. 273.
[23] P. Hamm, M. Lim, and R. M. Hochstrasser, in *Springer Series in Chemical Physics*, edited by T. Elsaesser, J. Fujimoto, D. Wiersma, and W. Zinth (Springer-Verlag, Berlin, 1998), Vol. 63, pp. 514–516.
[24] S. Mukamel, *Principles of Nonlinear Optical Spectroscopy* (Oxford University Press, New York, 1995).
[25] E. Backus, S. Garrett-Roe, and P. Hamm, Opt. Lett. **33**, 2665 (2008).
[26] P. Hamm, R. A. Kaindl, and J. Stenger, Opt. Lett. **25**, 1798 (2000).
[27] V. Volkov, R. Schanz, and P. Hamm, Opt. Lett. **30**, 2010 (2005).
[28] E. C. Fulmer, P. Mukherjee, A. T. Krummel, and M. T. Zanni, J. Chem. Phys. **120**, 8067 (2004).
[29] J. Bredenbeck and P. Hamm, Rev. Sci. Instrum. **74**, 3188 (2003).
[30] F. Delaglio, S. Grzesiek, G. W. Vuister, G. Zhu, J. Pfeifer, and A. Bax, J. Biomol. NMR **6**, 277 (1995).
[31] J. D. Hybl, A. W. Albrecht, S. M. G. Faeder, and D. M. Jonas, Chem. Phys. Lett. **297**, 307 (1998).
[32] A. D. Bristow, D. Karaiskaj, X. Dai, and S. T. Cundiff, Opt. Express **16**, 18017 (2008).
[33] D. Keusters, H.-S. Tan, and W. S. Warren, J. Phys. Chem. A **103**, 10369

(1999).
[34] A. Tokmakoff, J. Chem. Phys. **105**, 1 (1996).
[35] A. Tokmakoff, J. Chem. Phys. **105**, 13 (1996).
[36] K. Tominaga and K. Yoshihara, Phys. Rev. Lett. **74**, 3061 (1995).
[37] T. Steffen and K. Duppen, Phys. Rev. Lett. **76**, 1224 (1996).
[38] A. Tokmakoff, M. J. Lang, D. S. Larsen, G. R. Fleming, V. Chernyak, and S. Mukamel, Phys. Rev. Lett. **79**, 2702 (1997).
[39] D. J. Ulness, J. C. Kirkwood, and A. C. Albrecht, J. Chem. Phys. **108**, 3897 (1998).
[40] D. A. Blank, L. J. Kaufman, and G. R. Fleming, J. Chem. Phys. **111**, 3105 (1999).
[41] D. A. Blank, L. J. Kaufman, and G. R. Fleming, J. Chem. Phys. **113**, 771 (2000).
[42] K. J. Kubarych, C. J. Milne, and R. J. D. Miller, Int. Rev. Phys. Chem. **22**, 497 (2003).
[43] C. J. Milne, Y. L. Li, T. la Cour Jansen, L. Huang, and R. J. D. Miller, J. Phys. Chem. B **110**, 19867 (2006).
[44] E. C. Fulmer, F. Ding, and M. T. Zanni, J. Chem. Phys. **122**, 034302 (2005).
[45] O. Golonzka, N. Demirdöven, M. Khalil, and A. Tokmakoff, J. Chem. Phys. **113**, 9893 (2000).
[46] M. Cho, G. R. Fleming, and S. Mukamel, J. Chem. Phys. **98**, 5314 (1993).
[47] M. Cho, M. Du, N. F. Scherer, G. R. Fleming, and S. Mukamel, J. Chem. Phys. **99**, 2410 (1993).